

# Lipid-like biofilm from a clinical brain isolate of *Aspergillus terreus*: quantification, structural characterization and stages of the formation cycle.

**Gerardo Rayón-López**

Instituto Politécnico Nacional Escuela Nacional de Ciencias Biológicas: Instituto Politecnico Nacional Escuela Nacional de Ciencias Biologicas

**Natalee Carapia-Minero**

Instituto Politécnico Nacional Escuela Nacional de Ciencias Biológicas: Instituto Politecnico Nacional Escuela Nacional de Ciencias Biologicas

**María Gabriela Medina-Canales**

Instituto Politécnico Nacional Escuela Nacional de Ciencias Biológicas: Instituto Politecnico Nacional Escuela Nacional de Ciencias Biologicas

**Blanca Estela García-Pérez**

Instituto Politécnico Nacional Escuela Nacional de Ciencias Biológicas: Instituto Politecnico Nacional Escuela Nacional de Ciencias Biologicas

**Jesús Reséndiz-Sánchez**

Hospital Infantil de México Federico Gómez: Hospital Infantil de Mexico Federico Gomez

**Néstor O. Pérez**

Probiomed SA de CV

**Aida Verónica Rodríguez-Tovar**

Instituto Politécnico Nacional Escuela Nacional de Ciencias Biológicas: Instituto Politecnico Nacional Escuela Nacional de Ciencias Biologicas

**Adrián Ramírez Granillo** (✉ [adramirezg@ipn.mx](mailto:adramirezg@ipn.mx))

Instituto Politécnico Nacional Escuela Nacional de Ciencias Biológicas: Instituto Politecnico Nacional Escuela Nacional de Ciencias Biologicas <https://orcid.org/0000-0002-9399-6964>


---

## Research Article

**Keywords:** *Aspergillus terreus*, invasive aspergilosis, fungal biofilm, microhyphaes, lipid-like biofilm.

**Posted Date:** September 9th, 2022

**DOI:** <https://doi.org/10.21203/rs.3.rs-2000080/v1>

**License:**  This work is licensed under a Creative Commons Attribution 4.0 International License. [Read Full License](#)

# Abstract

Invasive infections caused by filamentous fungi have increased considerably due to the alteration of the host's immune response. Recently, *Aspergillus terreus* is considered an emerging pathogen and has shown resistance to amphotericin B treatment, resulting in high mortality. The development of fungal biofilm is a virulence factor, and it has been described in some cases of invasive aspergillosis. In addition, although the general composition of fungal biofilms is known, findings related to biofilms of a lipid nature are rarely reported. In this study, we present the identification of a clinical strain of *A. terreus* by microbiological and molecular tools, also its *in vitro* biofilm development capacity: i) Biofilm formation was quantified by Crystal Violet (CV) and reduction of tetrazolium salts assays (MTT), and simultaneously the stages of biofilm development were described by Scanning Electron Microscopy in High Resolution (SEM-HR). ii) Characterization of the organizational structure of the biofilm was performed by SEM-HR. The hyphal networks developed on the surface, the abundant air channels created between the ECM (extracellular matrix) and the hyphae fused in anastomosis were described. Also, the presence of microhyphae is reported. iii) The chemical composition of the ECM was analyzed by SEM-HR and CLSM (Confocal Laser Scanning Microscopy). Proteins, carbohydrates, nucleic acids and a relevant presence of lipid components were identified. Some structures of apparent waxy appearance were highlighted by SEM-HR and backscatter-electron diffraction, for which CLSM was previously performed. To our knowledge, this work is the first description of a lipid-type biofilm in filamentous fungi, specifically of the species *A. terreus* from a clinical isolate.

# Introduction

The *Aspergillus* group is made up of over 350 species. They are found in the soil as saprobes, but also cause diseases in plants, animals, and humans. This fungus demonstrates a series of adaptation mechanisms contained in its genome, which allow it to survive as a saprobiont and as a successful pathogen in human beings [1, 2]. *Aspergillus fumigatus*, *A. flavus*, *A. niger* and *A. terreus* are known for causing invasive aspergillosis (IA); however, *A. fumigatus* is the most frequent etiological agent. Specifically, in the case of *A. terreus*, which is integrated in the Terrei section, it is scarcely isolated from hosts that are undergoing some type of aspergillosis [55]. Epidemiologically, a clinical incidence of 4% of all IA due to this emerging fungus has been reported [56]. Likewise, the prevalence of IA caused by *A. terreus* is estimated to be between 15% and 23% in patients with hematologic malignancies [3]. In addition, the mortality rate is of concern since the immunosuppression factors of the patients are determinant for the invasive form of infection by this fungal species. At the same time, the clinical isolated frequently show resistance to first choice antifungal drugs (such as amphotericin B); moreover, the patients with a severe and prolonged neutropenia state show the absence of a therapeutic response with high mortality rate (51%-86%) [3, 4, 56]. The development of a biofilm for the genus *Aspergillus* has been reported to be a virulence factor favoring establishment and persistence of infection in the host [5, 6]. In the development and establishment of the biofilm, the differential expressions of genes implicated in the production of the extracellular matrix (ECM) have been reported [7], as well as during the conidial morphogenesis, which involves the change of the conidia into germinating tubes with an apical grown for the creation of hyphal networks. The biofilm allows the fungus to interact with the host, increasing the resistance to antifungal drugs (in part associated with the functionality of the efflux

pumps). In addition, the study of biofilm formation allows to analyze and propose the development of the pathogenesis of aspergillus infection, focusing mainly on possible therapeutic targets to control the infectious process, together with the ability of the fungus to evade the host immune response [3, 6].

In the present work, biofilm formation was analyzed and quantified by Crystal Violet (CV) and reduction of tetrazolium salts (MTT) assays. Simultaneously, the stages of biofilm development and characterization of the organizational structure of the biofilm were performed by SEM-HR (Scanning Electron Microscopy in High Resolution). Furthermore, the hyphal networks developed on the surface, the abundant air channels created between the extracellular matrix and the fused hyphae in anastomosis were described. Also, the presence of microhyphae rarely reported in filamentous fungi biofilm is reported. Moreover, by using SEM-HR and backscatter-electron diffraction, some structures of apparent waxy appearance were highlighted. Finally, the study was complemented by the analysis of the chemical composition of the ECM by Confocal Laser Scanning Microscopy (CLSM); proteins, carbohydrates, nucleic acids and a relevant presence of lipid components were identified. Data obtained on the chemical composition of the ECM are of special interest in filamentous fungi, since there are no reports on lipid synthesis in biofilms. Knowledge of the biofilm of *A. terreus* has multiple applications from the medical, agricultural, and biotechnological point of view. Therefore, this study opens a new research topic related to the virulent factors and possible treatments of and emerging pathogen [5–7].

## Materials And Methods

### Biological Material.

A clinical strain of *Aspergillus terreus*, was isolated from a pediatric patient with cerebral aspergillosis in the Mycology Laboratory of the Hospital Infantil de México "Federico Gómez" (HIMFG). The isolate was cultured and preserved on Potato Dextrose Agar (PDA) medium (BD Bioxon, Mexico) at 37°C.

### Microbiological and Molecular Identification.

The microbiological identification of *A. terreus* was carried out following the description made by Pasqualotto [8]. Colonial morphology was obtained on PDA and Sabourad Dextrose Agar (SDA), both cultures were incubated at 28 and 37°C for 1 to 7 days. In the description of microscopic morphology, the characteristics of the species were evaluated from a microculture incubated for 2 weeks on PDA medium.

Regarding molecular identification, deoxyribonucleic acid (DNA) was obtained through the method described by Rodríguez-Tovar *et al.* [63], from an *A. terreus* culture developed in a PDA medium, incubated during 7 days at 37°C. The DNA was quantified (Nanodrop 2000 Thermofisher®), adjusting the concentration to 100 ng/μL. Subsequently, the rRNA's ITS (Internal Transcript Spacer) molecular marker and the RNA polymerase II (RPBII) subunits were amplified by polymerase chain reaction (PCR) (MAXYGEN® brand thermocycler). The two molecular markers were amplified using the initiators described mainly for the *Aspergillus* species [10, 11, 12]. The reaction mixture was carried out for a final volume of 50 μL using TaqPol 5U/μL (Thermofisher®), MgCl<sub>2</sub> 3 mM, dNTP mixture 0.2 mM, 20 pmol of each initiator and sterile distilled water. The amplification protocol included a first denaturation cycle at 95°C for 5 minutes, followed by 30 cycles at

95°C/1 min, 55°C/1 min, and 72°C/1 min, with a final polymerization cycle at 72°C for 10 minutes. The products were sequenced by MACROGEN®. The sequences were analyzed with the SeaView program, and a concatenated phylogenetic tree was built using the MEGA 7.0 program to obtain the taxonomic position of the isolate.

### **Formation and quantification of *A. terreus* in vitro biofilm by CV and MTT assays.**

The biofilm was developed in polystyrene microplates (Nunk Roskilde, Denmark). Conidia were extracted by the method described by Mowat [13] to obtain the biofilm, which were then suspended in a Roswell Park Memorial Institute (RPMI)-1640 medium (Gibco, Waltham, MA, USA) supplemented with 2% glucose to a final concentration of  $4 \times 10^5$  conidia/mL [15]. The biofilm was developed adding 200  $\mu$ L of the conidia suspension to each of the wells in the 96-well plates, which were incubated at 37°C for 4 hours (adherence phase). The supernatant was eliminated with the purpose of removing the non-adhered cells, and 200  $\mu$ L of fresh RPMI medium were added. The plates were incubated during 24, 48, 72, and 96 hours at 37°C. The culture medium was eliminated and 200  $\mu$ L of the phosphate regulation solution 1X (PBS) were added to wash the wells. The quantification of the biofilm was carried out in accordance with the method described by Christensen [14] and modified by Ramírez-Granillo *et al.*, [15] using 0.005% violet crystal. The excess colorant was removed from the wells, which were washed with sterile distilled water and air-dried at room temperature. Finally, the colorant adhered to the biofilm was dissolved in 200  $\mu$ L of acetic acid (JT Baker, Phillipsburg, NJ, USA) at 33% (v/v). The solution was transferred to 96-well clean microplates and the absorbance was read at 595 nm in a spectrophotometer (Multiskan Ascent Thermo Labsystems, AIE, Waltham, MA, USA). The absorbance values are proportional to the amount of biofilm developed. This data was evaluated by the respective statistic methods described in the following paragraphs. To quantify the biofilm developed by determining its metabolic activity, the technique described by Walencka *et al.* [16], modified by Ramírez-Granillo *et al.*, was used [15, 57]. The biofilm was developed in 96-well polystyrene plates with a flat bottom, as described previously. 150  $\mu$ L of PBS 1X and 50  $\mu$ L of the tetrazolium salts reagent at 0.3% MTT [Bromide 3-(4,5-dimethylthiazol-2)-2,5-diphenyltetrazolium bromide] (SIGMA®, St. Louis, MO, USA) were added to each well. The plates were incubated during 2 hours at 37°C. Then, the MTT reagent was removed and 150  $\mu$ L of DMSO (Riedel-de Haën™, Seelze, Germany) and 25  $\mu$ L of glycine buffer 0.1 M at pH 10.2 (SIGMA®, St. Louis, MO, USA) were added. The plates were incubated during 15 minutes at room temperature stirring softly; the optical density was read with an ELISA reader (Multiskan Ascent Thermo Labsystems; AIE, Waltham, MA, USA) at 570 nm. The well with PBS 1X was used as a reagent blank. In this assay, twelve repetitions of three individual experiments were carried out, and the corresponding statistical analysis was performed with the data obtained.

### **Biofilm analysis through Scanning Electron Microscopy in High Resolution (SEM-HR).**

The biofilm was developed as described previously, and adjusted to 12-well polystyrene plates, incubated at 37°C during 24, 48, 72 and 96 hours. The SEM samples were processed in accordance with the method described by Bozzola and Russell, along with the protocols used by Vázquez-Nin and Echeverría [18, 19]. The biofilms were washed with PBS 1X and fixed with 2% glutaraldehyde (Electron Microscopy Sciences®, Washington, PA.) for 2 hours. A post-fixing was carried out with 1% osmium tetroxide (Electron Microscopy Sciences®, Washington, PA.) for 2 hours. Then, the intact biofilm was recovered from the bottom of the 12-

well plates. The samples were dehydrated with 10 to 90% ethanol during 10 minutes for each solution, respectively, and thrice with absolute ethanol for 10 minutes. The humidity in the biofilms was eliminated with a dryer, and they were dried to a critical point with hexamethyldisilazane (Electron Microscopy Sciences®, Washington, PA, USA). The samples were covered with a gold/palladium alloy during 400 seconds at 15,000 KV and 10  $\mu$ A; and were observed in a scanning electron microscope (JEOL, Tokyo, Japan) in the Nanosciences and Micro Nanotechnologies Center at the IPN.

### **Biofilm Structural Composition Analysis through CLSM.**

For the Confocal Laser Scanning Microscopy, the biofilms were developed as described previously. Glass coverslips (Velab, Mexico City, Mexico) were placed on the bottom of the 12-well plates. The biofilms were incubated during 72 and 96 hours at 37°C. The coverslips with the biofilm were recovered and placed in fluorochrome mixtures on glass slides. The mixtures were as follow: Calcofluor white (CW) 1 g/L (Sigma-Aldrich St. Louis, MO, USA) to tag the chitin; FUN®1 10 mM (Life Technologies, Gaithersburg MD, USA); for the metabolic activity; Concanavalin A (conA) 1 mg/mL (Sigma-Aldrich St. Louis, MO, USA) for glucose and mannose residues; Nile Red 10 mg/mL (Sigma-Aldrich St. Louis, MO, USA) for lipids; and Flamingo® 10X (Bio-Rad Laboratories Richmond, CA, USA) for proteins. In order to observe the samples, a Laser Confocal Scanning Microscope (Carl Zeiss, Germany) was used, the following filters were used: 480–530 nm (FUN®1), 355–433 nm (CW), 495–519 nm (conA), 514–650 nm (Nile Red) and 512–535 nm (Flamingo). The images were processed with the Zeiss LSM Image Browser ver. 4.0 software program (Carl Zeiss, Germany).

## **Statistical Analysis.**

Statistical analyses were based on the characteristics proposed by Ramírez-Granillo *et al.* (2015) and Allkja *et al.*, (2020) [15, 62]. The absorbance unit (AU) values obtained were analyzed by two-way ANOVA with the Student Neumals Kewls method for multifactorial analysis of variances. SigmaPlot ver.12.0 software (Systat Software Inc., San Jose, CA, USA) was used for statistical analysis.

## **Results**

### **Microbiological and Molecular Identification.**

The clinical isolate was identified as the *Aspergillus terreus* filamentous fungus. The molecular identification was performed with the analysis of sequences obtained from the ITS fragment and the RPBII subunit as molecular marker using species closely related to the genus *Aspergillus*. The identity of the fungal isolate was confirmed with the concatenated phylogenetic tree for *A. terreus* species (Fig. 1a) and is related to section Terrei. The characteristics of the *A. terreus* species in a PDA medium were described. The radial colony was observed with a phenotype typical of the species (granular texture, flat surface with production of white pigment at the periphery and eventually darkening to brown). On the reverse side plate, a brown pigment, and a yellow pigment diffusible to the medium were formed (Fig. 1b). Similarly, at the microscopic level, the characteristic structures of *A. terreus* were observed. The morphology of the *A. terreus* conidial head was subspherical, and two series of phialides originate from the conidiophore at an angle of approximately 180°, with a chain arrangement of columnar conidia (Fig. 1c). Furthermore, the effect of incubation

temperature (28°C and 37°C) and the composition of the culture medium (SDA or PDA) on fungal growth were analyzed. Regarding the diameter of colonies developed at 28°C, no significant differences were observed between PDA and SDA medium (Online Resource 1a). Likewise, at 37°C, a statistically significant difference was observed in the PDA medium (Online Resource 1b) in the diameter of fungal colonies during a 7-day incubation period.

### **Quantification of *A. terreus* in vitro biofilm.**

The ability to develop biofilm *in vitro* for *A. terreus* clinical isolate, under different growth conditions (temperature, conidial concentration, and incubation time) was evaluated. The kinetics of biofilm showed that the optimum temperature and the highest biofilm production occurred at 37°C with a concentration of  $4 \times 10^5$  conidia/mL (results not shown). Quantification of the *A. terreus* biofilm was performed by Christensen-Crystal Violet (CV-biomass) and tetrazolium salt reduction (MTT-metabolic activity) methods described by Walencka [16]. Additionally, the characteristics of the biofilm of the filamentous fungus were described by SEM-HR (Fig. 2). By CV method, growth kinetics data were shown with the highest amount of biofilm developed at 72 hours (AU > 2.0) (Fig. 2a). The highest metabolic activity of the fungus was detected at 24 hours of *in vitro* biofilm development (AU > 0.7) (Fig. 2b). Correlating the structure of the *A. terreus in vitro* biofilm by SEM-HR with the amount evaluated, the typical characteristics of filamentous fungal biofilm (abundant hyphal growth, development of air channels and anastomosis) were visualized (Fig. 2c). First, a hyphal network was observed at 24 hours with ECM extensively covering the colonized surface, according to CV analysis (AU < 2.0), and high metabolic activity (AU > 0.7). Then, the number of hyphae decreased along with the presence of ECM at 48 hours, like what was quantified previously (CVM, AU > 1.5; MTT, AU < 0.6). After 72 hours of incubation, biofilm fields with a high biomass density were observed (AU > 2.0), and no surface on which the fungus adhered was evident. Also, the metabolic activity of this biofilm formation time was elevated (MTT, AU < 0.8). During the 96-hour period, a decrease in the fungal population was observed, with some remnants of the biofilm developing (Fig. 2c). The quantification of the biomass at this time was determined with a value of AU  $\approx$  0.4 and a MTT value of AU > 0.3.

### **Stages of *A. terreus* biofilm formation.**

The establishment during the first hours of the biofilm of the filamentous fungus has been described as adhesion processes, cell aggregation, exopolymeric substance (EPS) production and development of biofilm formation (Fig. 3a). For each stage of the fungal biofilm, the presence of typical characteristics at previously quantified times was described (Table 1). The biofilm *in vitro* formation cycle, after the first hours of establishment, for the clinical isolate of *A. terreus* was described by SEM-HR as shown below:

- **Early maturation stage (24 hours).**

The formed biofilm was observed to initiate the early maturation phase with predominant hyphal networks forming anastomosis, and abundant air channels between the produced ECM (Fig. 3b). In addition, only during this phase were structures called microhyphae visualized with a diameter of  $\approx$  1  $\mu$ m and a shorter length compared to a standard size hypha (> 10  $\mu$ m). Several scattered microhyphae with catenular organization adjacent to the ECM and fused hyphae were observed in the biofilm (Fig. 3c).

- **Depletion stage (48 hours).**

At this stage, different organizations of the ECM were observed. First, a condensed porous structure with embedded hyphae was visualized (Fig. 3d), along with structural arrangements resembling a coral of waxy aspect (Fig. 3e). In another field, a porous ECM with adjacent hyphae (Fig. 3f), and globular arrangements were observed at the periphery of the ECM (Fig. 3g). Notably, a decreasing fungal biomass with few canals and anastomoses was observed.

- **Late maturation stage (72 hours).**

At this stage, extracellular complexes with a condensed ECM and embedded organized hyphae were observed massively covering the abiotic surface (Fig. 3h). In addition, several air channels and stable anastomosed hyphae were observed among the fungal biofilm (Fig. 3i). Also, further biofilm development was shown with prominent porous ECM formations covering the developed hyphae (Fig. 3j).

- **Dispersion stage (96 hours).**

A weak biofilm with low biomass and wide spaces between hyphae was observed. The deficit of ECM production was evident, as well as the scarce presence of aerial canals (Fig. 3k). In some sample fields, ECM residues were observed with fragments of sectioned hyphae enveloped by a layer of EPS secreted by the filamentous fungus (Fig. 3l). During this stage, several asexual structures (conidia) were observed aggregated or isolated (Fig. 3m, 3n).

### **Analysis of the biofilm structural composition of a clinical isolate of *A. terreus* by CLSM and SEM-HR.**

The composition of EPS composing the ECM of the biofilm *in vitro* was detected by CLSM. At 24 and 48 h, glucose and mannose residues were observed in CW- and Con-A-labeled hyphae. These cells were metabolically active, as they overlapped with the staining corresponding to FUN 1. Blue halo cells labeled with Flamingo for proteins were also observed (Data not shown). The most representative results were obtained at 72 and 96 hours. In general, the micrographs analyzed (Fig. 4a, 4b); an intense mark was detected along the hyphal wall, related to the chitin (CW - green halo). Likewise, together with this signal, several halos were detected in the hyphae related to the secretion of molecules of lipid nature (Nile red - pink halo). At 72 hours (Fig. 4a), we observed a moderate secretion of lipids in the *in vitro* biofilm development kinetics, compared to 96 hours in which showed a higher amount of these molecules (Fig. 4b). Furthermore, the co-localization of carbohydrate and lipid labeling molecules was noted in the biofilm of *A. terreus* (Fig. 4c).

SEM-HR micrographs of the biofilm at 96 hours were analyzed showing evidence of fields exhibiting faceted bodies (similar to a polyhedral structure) (Fig. 4d). These foreign bodies were denominated waxy ECM (Fig. 4e), due to their appearance and texture. Further studies will be able to define if their origin is indeed lipidic; but, under the microscope, it was observed to be secreted by the hyphae of the filamentous fungus. To determine that this fungal biofilm structure was derived from the hyphae, SEM-HR analysis with backscatter-electron diffraction was performed. Finally, crystallographic structures of the material were shown to be part of the waxy ECM of the fungus secreted by the hyphae (Fig. 4f).

## Discussion

The genus *Aspergillus* consists of four sections: Fumigati (*A. fumigatus*), Nigri (*A. niger*), Terrei (*A. terreus*) and Flavi (*A. flavus*). Currently, there are  $\approx 16$  species accepted in section Terrei [8, 20, 21, 55]. In recent years, medical interest in *A. terreus* has been related to its role as an emerging opportunistic pathogen causing invasive aspergillosis (IA) in immunocompromised patients, such as individuals with severe neutropenia for prolonged periods, cancer patients, bone marrow transplant recipients and those undergoing immunosuppressive therapy [55]. The largest number of cases of *A. terreus* resistant to amphotericin B treatment is reported from India [21, 22]. Regarding the clinical forms of IA, central nervous system (CNS) aspergillosis is rare in Mexico. While worldwide, the main causative agents of aspergillosis are *A. fumigatus* and *A. flavus* [23, 24]. Epidemiologically, IA worldwide presents incomplete data that vary according to the study region. During the last few years, an increase in IA has been reported along with cases in immunocompromised patients [24], and at the same time, the mortality rate in patients acquiring this fungal infection has increased, although the incidence in recent decades has decreased [25].

CNS aspergillosis is commonly reported in Middle Eastern countries with dry climates (India and Saudi Arabia) [8, 26]. Additionally, cases of this clinical presentation caused by *A. terreus* are rare [27–29].

The clinical strain used in this study was isolated by the Hospital Infantil de México "Federico Gómez". The identity of the fungal agent was corroborated as *A. terreus*. The origin of the clinical isolate is from a pediatric patient with CNS aspergillosis. Although this is not a clinical report, it is important to mention that, to our knowledge, there are scarce reports of this IA caused by *A. terreus* in Mexico [24, 64].

Filamentous fungi of the genus *Aspergillus* are described as saprobes or opportunistic pathogens, and these behaviors are conditioned by multifactorial interactions such as host type, host immune status, fungal inoculum concentration, conidial diameter, climatic conditions, and the expression of virulence factors of each *Aspergillus* species [1, 13, 30]. Specifically for *A. terreus*, some virulence factors have been described [2, 30–35]. Additionally, *A. terreus* is related to its ability to develop a biofilm [30, 36], although it has not been described in detail at the quantitative and structural level.

The development of a biofilm is a common process among filamentous fungi for their establishment, survival, and colonization in nature, as well as in specific hosts. Additionally, the importance of the study of fungal *in vitro* biofilm provides information that can be applied in fields such as clinical practice, organ, and tissue engineering or in the study of infectious processes. In the industrial field, some studies indicate that biofilms adhere to pipes and inert surfaces, causing economic losses in manufacturing processes [37, 38]. The data obtained in this research have made it possible to describe the stages of *in vitro* biofilm formation. It was shown that around 24 hours an early maturation occurs, and around 48 and 72 hours respectively, a decrease in the biofilm formed with a statistically representative later elevation was shown. Likewise, it is possible to link a similar behavior to the logarithmic phase and the lag phase (adaptation) in conventional microbial growth kinetics, like that described for *A. fumigatus* biofilm [41–44]. The decrease in fungal biofilm formation between 24 and 48 hours (Fig. 2a; Fig. 2b) could be considered a stress caused by the incubation temperature at 37°C (for *A. terreus* efficient colonial growth was determined at 28°C) (Online Resource 1a). Between 48 and 72 hours, the absorbance units increased in relation to the biofilm concentration. The reason



is because a process of co-aggregation of planktonic cells on the adherent layer of sessile hyphae was manifested. This behavior was shown in micrographs with abundant hyphae embedded in abundant ECM (Fig. 2c). Likewise, the lowest biofilm development was detected at 96 hours. This decrease in metabolic activity of *A. terreus* may be related to the dispersion phase described in filamentous fungi [40, 41]. The dispersal phase allows recolonization of other surfaces given the release of propagules, either hyphae or conidia, to restart the cycle. At the same time, cell death is imminent given the extensive development time; therefore, there is a decrease in fungal cell number and metabolic activity in the biofilm [40, 45, 46].

Otherwise, the architecture of fungal biofilms of *Aspergillus* species, except for *A. fumigatus*, has been described in a discrete manner. Particularly, in *A. terreus* there are no reports detailing the structure of its biofilm. In this study, the morphology of the biofilm of *A. terreus* was analyzed by SEM at different incubation times. Initially, abundant biomass (hyphae embedded in the ECM and germinating conidia) was observed in the 24-hour micrographs. This behavior was complementary to the result obtained by MTT assay (high fungal metabolic activity). In the fungal biofilm of *A. terreus*, structures known as microhyphae formed along anastomosed hyphae were observed at 24 h (Fig. 3b, Fig. 3c). The occurrence of these structures is usually rare. In the case of *A. terreus*, no microhyphae have been found, but for other *Aspergillus* species only microhyphae have been described in the biofilm of *A. fumigatus* [41]. Other reports on microhyphae in which these fungal structures predominate have been related to infections in plant tissues caused by some species of endophytic fungi such as *Ophiostoma ulmi*, *Phialocephala fortinii* and *Fusarium oxysporum* [58, 59, 60]. In human pathogens there are no reports demonstrating the existence of microhyphae, except for the role mentioned above on a clinical strain of *A. fumigatus* [41]. There has been an article mentioning the name of microhyphae in mycetoma infections caused by actinomycetes, but it refers to the description of microsiphonate mycelium [61]. However, the role of microhyphae has not been explained for the genus *Aspergillus*, apart from plant models. In *A. terreus*, other modified asexual structures (phialidic and globular accessory conidia) have been reported, attributing to them an invasion effect on the infected host, in combination with other fungal virulence factors. Future studies should focus on defining their role in the metabolism of the fungus [33].

Outstanding biofilm findings were also observed at 48 hours, accompanied by a decrease in biomass and metabolic activity of the fungus, comparable with SEM micrographs (Fig. 3d, 3f); at the same time, two types of extracellular matrix were observed: condensed-porous ECM (Fig. 3e) and vesicular ECM (Fig. 3g). Several types of ECM have been described in the *in vitro* biofilm model of *A. fumigatus*, such as porous-type ECM, dense-type ECM and film-type ECM. The cause of the presence of these ECM was related to the antibiosis manifested by the fungus-bacteria interaction with *S. aureus* [15]. For the diversity of ECM structures in *A. terreus*, probably it is related to the lipids produced in the biofilm. A waxy like matrix appearance of condensed and porous ECM was observed (Fig. 3e).

Likewise, in the micrographs obtained at 72 hours, in comparison with the quantitative analysis obtained from highest biomass production, the characteristics of biofilm patterns were verified (Fig. 2c; Fig. 3h). An ECM with abundant embedded mycelium was observed, and in the same fields several types of extracellular matrix: condensed ECM, film-like ECM (Fig. 3i) and vesicular ECM (Fig. 3j). Particularly, a comparison of film-like ECM of *A. terreus* showed similar characteristics to those described for the biofilm of *A. fumigatus* [15].

Once described, the biofilm of *A. terreus* at 72 h of incubation was compared with stage V of the filamentous fungal biofilm model proposed by Harding *et al.* [40]. And it also relates to the maturation stage of the *A. fumigatus* biofilm model that was observed by González-Ramírez *et al.* [41]. Furthermore, this result is also similar to that reported by Wuren *et al.*, since despite having different culture conditions; they detected a mature biofilm between 24 and 72 hours [36].

During 96 hours of biofilm development, sparse hyphae were observed by SEM, comparable to a decrease in absorbance units statistically verified by CV and MTT when quantifying the biofilm (Fig. 2). Although the characteristics of a functional fungal biofilm (hyphal anastomosis, canals, and ECM) were maintained at 96 hours, it can be assumed that this is the dispersal phase of the *A. terreus* biofilm (Fig. 3k; Fig. 3m). This deduction was derived from the phase VI proposed in the fungal biofilm model and the dispersal phase of *A. fumigatus* in which the shedding of reproductive structures, either hyphae or conidia, occurs [40, 41]. The restart of the biofilm production cycle during this phase explains the decrease of mycelium in several fields, although it is possible to observe developing conidia during this final phase of the fungal biofilm (Fig. 3m; Fig. 3n).

Afterwards, to know the chemical composition of ECM, CLSM technique was used on the *in vitro* biofilm of *A. terreus* at 72 and 96 h, to detect chitin and lipids. All the most representative signals were observed in the biofilms at these incubation times when labeled with the specific fluorochromes as calcofluor white (green halo); it was repeated for both incubation times. Moreover, lipids were labeled with Nile Red (purple halo). The signal was highest at 96 hours and co-localized with the green halos of chitin (Fig. 4a; Fig. 4b). Previous studies have reported the role of carbohydrates in the biofilm structure, whose function is linked to providing stability and integrity due to hydrophilic polysaccharides that maintain the hydration of the biofilm, preventing desiccation and capturing water from the medium in the biofilm. Probably, this function is also carried out in the biofilm of *A. terreus* [6, 15, 46–48]. The lipid content among the structural components of the ECM in *A. terreus* was unexpected, as these constituents have not been described in filamentous fungal biofilms. Therefore, the detection of lipids with the fluorochrome Nile Red was shown that the biofilm is formed of significant amounts of these molecules given the intensity and number of homogeneous purple halos tagged practically in all hyphae (Fig. 4a; Fig. 4b; Fig. 4c). Prior to this, other microscopy techniques were used to elucidate the existence of lipids in the biofilm, as proved by CLSM. While analyzing some SEM micrographs of the fungal biofilm, specifically at 96 hours, wax-like icosahedral faceted structures (referred to as ECM wax) were observed adjacent to the hyphae (Fig. 4d; Fig. 4e). To analyze the crystallographic patterns of some of the biofilm components, the backscatter electron diffraction technique was used. Under this microscopic analysis, the reasoning is focused on detecting some type of reflective effect in the faceted structure that differs from the bio-organic crystalline pattern of the fungus; in the case of a non-hyphal component, such as a metal [49, 50]. Finally, the hyphae and the waxy ECM showed a similar crystallographic pattern, so it was considered that the fungus secreted this exopolymeric material (Fig. 4f). Presumably, the production of these polyhedral structures showing a waxy appearance is related to the scarcity of hyphae on the surface and the secreted lipid composition (also detected with CLSM). Similarly, the presence of poor lipids was reported when a condensed and porous ECM was observed at 48 hours (Fig. 3d-3g). Although these results of microscopic analysis are a first approximation to the lipid composition in filamentous fungal biofilms, and should be studied in detail, there are also evidences of the synthesis of

molecules of this nature in these fungal species. Based on this finding of the description of lipid constituents in the ECM, it should be mentioned that *A. terreus* was used at the biotechnological level to produce lovastatin [competitive inhibitor of 3-hydroxy-3-methylglutaryl-coenzyme A reductase (HMG-CoA)]. This enzyme was involved in the synthesis of mevalonate, an intermediate metabolite in the synthesis of ergosterol (main components of the fungal membrane) and cholesterol. Thus, since lovastatin has a lipid origin (statin family), it could be related to the ergosterol synthesis pathway [31, 43, 51, 52, 55]. Currently, this could be the answer to the increase in lipid production at 96 h of incubation of the *A. terreus* biofilm in this work.

This study presents a series of findings, which are important given the scope of applications that can be handled in the short and long period in the clinical, epidemiological, pharmaceutical, and microbiological fields. These perspectives can be focused on the search for therapeutic targets, biological control and containment for a fungal agent that has been rarely isolated in México and is beginning to manifest itself in several clinical cases of this filamentous fungus on a worldwide scale [51, 53, 54]. Finally, the most important aspects observed during the development of the *in vitro* biofilm of *A. terreus* were the following: i) the stages of biofilm development were described; ii) the organizational structure of the biofilm was characterized, reporting the presence of microhyphae, previously unreported for this species; and iii) the chemical composition of the ECM was analyzed, demonstrating a relevant content of lipid components. To our knowledge, this work is the first description of a lipid-type biofilm in filamentous fungi, specifically of the species *A. terreus* from a clinical isolate. Moreover, this study is the first to show the identification of a clinical isolate of *A. terreus*, the cause of cerebral aspergillosis in our country, as well as to demonstrate the ability of this isolate to develop an *in vitro* biofilm and the characterization of them.

## Declarations

### Funding.

This work was supported by Instituto Politécnico Nacional, Mexico City [SIP20210778, SIP20210200, SIP20220564, SIP20221965]. Author GRL has receives research support from BEIFI/Instituto Politécnico Nacional. Authors AVRT and ARG have received research support from EDI, COFAA/Instituto Politécnico Nacional and SNI/CONACYT México.

### Competing interests.

The authors declare no conflicts of interest.

### Author Contributions.

All authors contributed to the study conception and design. Material preparation, data collection and analysis were performed by Gerardo Rayón-López, Natalee Carapia-Minero, María Gabriela Medina-Canales, Blanca Estela García-Pérez, Jesús Reséndiz-Sánchez, Néstor O. Pérez, Aída Verónica Rodríguez-Tovar and Adrián Ramírez-Granillo. The first draft of the manuscript was written by Gerardo Rayón-López and all authors commented on previous versions of the manuscript. All authors read and approved the final manuscript.

## References

1. Tekaia F, Latgé JP. *Aspergillus fumigatus*: saprophyte or pathogen? *Curr Opin Microbiol*. 2005;8(4):385–92. <https://doi.org/10.1016/j.mib.2005.06.017>.
2. Kwon-Chung KJ, Sugui JA. *Aspergillus fumigatus*-What makes the species a ubiquitous human fungal pathogen? *PLoS Pathog*. 2013;9(12):e1003743. <https://doi.org/10.1371/journal.ppat.1003743>.
3. Hachem R, Gomes MZ, El Helou G, El Zakhem A, Kassis C, Ramos E, Jiang Y, Chaftari AM, Raad II. Invasive aspergillosis caused by *Aspergillus terreus*: an emerging opportunistic infection with poor outcome independent of azole therapy. *J Antimicrob Chemother*. 2014;69(11):3148–55. <https://doi.org/10.1093/jac/dku241>.
4. Tritz DM, Woods GL. Fatal Disseminated Infection with *Aspergillus terreus* in Immunocompromised Hosts. *Clin Infect Dis*. 1993;16(1):118–22. <https://doi.org/10.1093/clinids/16.1.118>.
5. Mowat E, Williams C, Jones B, McChlery S, Ramage G. The characteristics of *Aspergillus fumigatus* mycetoma development: is this a biofilm? *Med Mycol*. 2009;47(Suppl 1):120–6. <https://doi.org/10.1080/13693780802238834>.
6. Rajendran R, Mowat E, McCulloch E, Lappin DF, Jones B, Lang S, Majithiya JB, Warn P, Williams C, Ramage G. Azole resistance of *Aspergillus fumigatus* biofilms is partly associated with efflux pump activity. *Antimicrob Agents Chemother*. 2011;55(5):2092–7. <https://doi.org/10.1128/AAC.01189-10>.
7. Branda SS, Vik A, Friedman L, Kolter R. Biofilms: the matrix revisited. *Trends Microbiol*. 2005;13:20–6. <https://doi.org/10.1016/j.tim.2004.11.006>.
8. Guarro J, Orzechowski M, Severo X, Severo LC. Differences and Similarities Amongst Pathogenic *Aspergillus* Species. In: Pasqualotto AC, editor. *Aspergillosis: From Diagnosis to Prevention*. Porto Alegre, Brazil: Springer; 2010. pp. 7–32. <https://doi.org/10.1007/978-90-481-2408-4>.
9. Allers T, Lichten M. A method for preparing genomic DNA that restrains branch migration of Holliday junctions. *Nucleic Acid Res*. 2000;28(2):e6. <https://doi.org/10.1093/nar/28.2.e6>.
10. Gardes M, Bruns TD. ITS primers with enhanced specificity for basidiomycetes-application to the identification of mycorrhizae and rusts. *Mol Ecol*. 1993;2(2):113–8. <https://doi.org/10.1111/j.1365-294x.1993.tb00005.x>.
11. Peterson SW. Phylogenetic analysis of *Aspergillus* species using DNA sequences from four loci. *Mycologia*. 2008;100(2):205–26. <https://doi.org/10.3852/mycologia.100.2.205>.
12. Tsang CC, Tang JYM, Lau SKP, Woo PCY. Taxonomy and evolution of *Aspergillus*, *Penicillium* and *Talaromyces* in the omics era – Past, present and future. *Comput Struct Biotechnol J*. 2018;16:197–210. <https://doi.org/10.1016/j.csbj.2018.05.003>.
13. Mowat E, Rajendran R, Williams C, McCulloch E, Jones B, Lang S, Ramage G. *Pseudomonas aeruginosa* and their small diffusible extracellular molecules inhibit *Aspergillus fumigatus* biofilm formation. *FEMS Microb Lett*. 2010;313(2):96–102. <https://doi.org/10.1111/j.1574-6968.2010.02130.x>.
14. Christensen GD, Simpson WA, Younger JJ, Baddour LM, Barrett FF, Melton DM, Beachey EH. Adherence of coagulase-negative staphylococci to plastic tissue culture plates: a quantitative model for the

- adherence of staphylococci to medical devices. *J Clin Microbiol.* 1985;22(6):996–1006.  
<https://doi.org/10.1128/jcm.22.6.996-1006.1985>.
15. Ramírez-Granillo A, Canales MG, Espíndola ME, Martínez Rivera MA, de Lucio VM, Tovar AV. Antibiosis interaction of *Staphylococcus aureus* on *Aspergillus fumigatus* assessed *in vitro* by mixed biofilm formation. *BMC Microbiol.* 2015;15:33. <https://doi.org/10.1186/s12866-015-0363-2>.
  16. Walencka E, Sadowska B, Rozalska S, Hryniewicz W, Rózsalska B. Lysostaphin as a potential therapeutic agent for staphylococcal biofilm eradication. *Pol J Microbiol.* 2005;54(3):191–200.
  17. Ramírez-Granillo A. Analysis of the antagonistic interaction between *Aspergillus fumigatus* and *Staphylococcus aureus* during biofilm formation. PhD thesis, Escuela Nacional de Ciencias Biológicas-Instituto Politécnico Nacional, 2017.
  18. Bozzola JJ, Russell LD. Specimen Preparation For Scanning Electron Microscopy. *Electron Microscopy: Principles and Techniques for Biologists.* 2nd ed. New York: Jones and Bartlett Press. 1999:pp. 48–71.
  19. Vazquez-Nin G, Echeverría. Introduction To The Electronic Microscopy Applied To The Biological Sciences, [Introducción a la microscopia electrónica aplicada a las ciencias biológicas]. CDMX: Fondo de Cultura Económica; 2000.
  20. Alastruey-Izquierdo A, Mellado E, Cuenca-Estrella M. Current section and species complex concepts in *Aspergillus*: recommendations for routine daily practice. *Ann N Y Acad Sci.* 2012;1273:18–24.  
<https://doi.org/10.1111/j.1749-6632.2012.06822.x>.
  21. Zoran T, Sartori B, Sappl L, Aigner M, Sánchez-Reus F, et al. Azole-Resistance in *Aspergillus terreus* and Related Species: An Emerging Problem or a Rare Phenomenon? *Front Microbiol.* 2018;9:516.  
<https://doi.org/10.3389/fmicb.2018.00516>.
  22. Kathuria S, Sharma C, Singh PK, Agarwal P, Agarwal K, Hagen F, Meis JF, Chowdhary A. Molecular Epidemiology and *In-Vitro* Antifungal Susceptibility of *Aspergillus terreus* Species Complex Isolates in Delhi, India: Evidence of Genetic Diversity by Amplified Fragment Length Polymorphism and Microsatellite Typing. *PLoS ONE.* 2015;10(3):e0118997. <https://doi.org/10.1371/journal.pone.0118997>.
  23. Marzolf G, Sabou M, Lannes B, Cotton F, Meyronet D, Galanaud D, Cottier JP, Grand S, Desal H, Kreutz J, Schenck M, Meyer N, Schneider F, Dietemann JL, Koob M, Herbrecht R, Kremer S. Magnetic Resonance Imaging of Cerebral Aspergillosis: Imaging and Pathological Correlations. *PLoS ONE.* 2016;11(4);  
[doi:10.1371/journal.pone.0152475](https://doi.org/10.1371/journal.pone.0152475).
  24. De Anda-Gómez MA, Díaz-Ponce H, Pacheco-Rosas DO, Reséndiz-Sánchez J, Sandoval-Mex AM. Diagnosis Of Invasive Aspergillosis In Children Under 18 Years Of Age, [*Diagnóstico de Aspergilosis Invasora en menores de 18 años de edad*]. CDMX, Mexico: Instituto Mexicano del Seguro Social. 2013.
  25. Cruz-Contreras DG. Invasive aspergillosis in the patient receiving an allogeneic hematopoietic progenitor cell transplant: epidemiology, diagnosis, prophylaxis and treatment, [Aspergilosis invasiva en el paciente que recibe trasplante alogénico de células progenitoras hematopoyéticas: epidemiología, diagnóstico, profilaxis y tratamiento]. *Rev Hematol Mex.* 2016;17(4):262–7.
  26. Vergara GE, Roura N, Del Castillo M, Mora A, Alcorta SC, Mormandi R, Cervio A, Salvat J. Cervical aspergillosis with dissemination to the central nervous system: Case reports and review of the literature.

- [Aspergilosis cervical con diseminación al sistema nervioso central. Presentación de un caso y revisión de bibliografía]. Surg Neurol Int. 2015;6(Suppl 20):524–9. <https://doi.org/10.4103/2152-7806.167203>.
27. Damek DM, Lillehei KO, Kleinschmidt-DeMasters BK. *Aspergillus terreus* brain abscess mimicking tumor progression in a patient with treated glioblastoma multiforme. Clin Neuropathol. 2008;27(6):400–7. <https://doi.org/10.5414/npp27400>.
  28. Elsayy A, Faidah H, Ahmed A, Mostafa A, Mohamed F. *Aspergillus terreus* Meningitis in Immunocompetent Patient: A Case Report. Front Microbiol. 2015;6:1353. <https://doi.org/10.3389/fmicb.2015.01353>.
  29. Srikumar T, Pabbathi S, Fernandez J, Nanjappa S. *Aspergillus Terreus* Brain Abscess Complicated by Tension Pneumocephalus in a Patient with Angiosarcoma. Am J Case Rep. 2017;18:33–7. <https://doi.org/10.12659/ajcr.900425>.
  30. Raksha SG, Urhekar AD. Virulence Factors Detection in *Aspergillus* Isolates from Clinical and Environmental Samples. J Clin Diagn Res 2017;11(7): DC13-DC18; <https://doi.org/10.7860/JCDR/2017/24055.10211>.
  31. Lass-Flörl C, Griff K, Mayr A, Petzer A, Gastl G, Bonatti H, Freund M, Kropshofer G, Dierich MP, Nachbaur D. Epidemiology and outcome of infections due to *Aspergillus terreus*: 10-year single centre experience. Br J Haematol. 2005;131(2):201–7. <https://doi.org/10.1111/j.1365-2141.2005.05763.x>.
  32. Thakur R, Shankar J. Proteome profile of *Aspergillus terreus* conidia at germinating stage: Identification of probable virulent factors and enzymes from mycotoxin pathways. Mycopathologia. 2017;182:771–84. <https://doi.org/10.1007/s11046-017-0161-5>.
  33. Bengyella L, Yekwa EL, Subhani MN, Tambo E, Nawaz K, Hetsa BA, Iftikhar S, Waikhom SD, Roy P. Invasive *Aspergillus terreus* morphological transitions and immunoadaptations mediating antifungal resistance. Infect Drug Resist. 2017;10:425–36. <https://doi.org/10.2147/IDR.S147331>.
  34. Won EJ, Choi MJ, Shin JH, Park YJ, Byun SA, Jung JS, Kim SH, Shin MG, Suh SP. Diversity of clinical isolates of *Aspergillus terreus* in antifungal susceptibilities, genotypes and virulence in *Galleria mellonella* model: Comparison between respiratory and ear isolates. PLoS ONE. 2017;12(10):e0186086. <https://doi.org/10.1371/journal.pone.0186086>.
  35. Shin WS, Lee D, Kim S, Jeong YS, Chun GT. Development of miniaturized culture systems for large screening of mycelial fungal cells of *Aspergillus terreus* producing itaconic acid. J Microbiol Biotechnol. 2017;27(1):101–11. <https://doi.org/10.4014/jmb.1610.10037>.
  36. Wuren T, Toyotome T, Yamaguchi M, Takahashi-Nakaguchi A, Muraosa Y, Yahiro M, Wang DN, Watanabe A, Taguchi H, Kamei K. Effect of serum components on biofilm formation by *Aspergillus fumigatus* and other *Aspergillus* species. Jpn J Infect Dis. 2014;67(3):172–9. <https://doi.org/10.7883/yoken.67.172>.
  37. Gutiérrez-Correa M, Ludeña Y, Ramage G, Villena GK. Recent Advances on Filamentous Fungal Biofilms for Industrial Uses. Appl Biochem Biotechnol. 2012;167(5):1235–53. <https://doi.org/10.1007/s12010-012-9555-5>.
  38. Kaur S, Singh S. Biofilm formation by *Aspergillus fumigatus*. Med Mycol. 2014;52:2–9. <https://doi.org/10.3109/13693786.2013.819592>.

39. Camarillo-Márquez O, Córdova-Alcántara IM, Hernández-Rodríguez C, García-Pérez BE, Martínez-Rivera M, Rodríguez-Tovar AV. Antagonistic Interaction of *Staphylococcus aureus* Toward *Candida glabrata* During *in vitro* Biofilm Formation Is Caused by an Apoptotic Mechanism. *Front Microbiol.* 2018;9:2031; <https://doi.org/10.3389/fmicb.2018.02031>.
40. Harding MW, Marques LL, Howard RJ, Olson ME. Can filamentous fungi form biofilms? *Trends microbiol.* 2009;17(11):475–80. <https://doi.org/10.1016/j.tim.2009.08.007>.
41. González-Ramírez AI, Ramírez-Granillo A, Medina-Canales MG, Rodríguez-Tovar AV, Martínez-Rivera MA. Analysis and description of the stages of *Aspergillus fumigatus* biofilm formation using scanning electron microscopy. *BMC Microbiol.* 2016;16(1):243. <https://doi.org/10.1186/s12866-016-0859-4>.
42. Kulkarni G. Introduction To Fermentation Technology. In: *Biotechnology And its applications in pharmacy*. New Delhi: Jaypee Brothers Medical Publishers Ltd; 2002. p. 7.
43. Srinivasan N, Thangavelu K, Uthandi S. Lovastatin production by an oleaginous fungus, *Aspergillus terreus* KPR12 using sago processing wastewater (SWW). *Microb Cell Fact.* 2022;21(1):22. <https://doi.org/10.1186/s12934-022-01751-2>.
44. Beauvais A, Schmidt C, Guadagnini S, Roux P, Perret E, Henry C, Paris S, Mallet A, Prévost MC, Latgé JP. An extracellular matrix glues together the aerial-grown hyphae of *Aspergillus fumigatus*. *Cell Microbiol.* 2007;9(6):1588–600. <https://doi.org/10.1111/j.1462-5822.2007.00895.x>.
45. Ramage G, Rajendran R, Gutiérrez-Correa M, Jones B, Williams C. *Aspergillus* biofilms: clinical and industrial significance. *FEMS Microb Lett.* 2011;324(2):89–97. <https://doi.org/10.1111/j.1574-6968.2011.02381.x>.
46. Fanning S, Mitchell AP. Fungal Biofilms. *PLoS Pathog.* 2012;8(4):e1002585. <https://doi.org/10.1371/journal.ppat.1002585>.
47. Flemming HC, Wingender J. The biofilm matrix. *Nat Rev Microbiol.* 2010;8(9):623–33. <https://doi.org/10.1038/nrmicro2415>.
48. Shopova I, Bruns S, Thywissen A, Kniemeyer O, Brakhage AA, Hillmann F. Extrinsic extracellular DNA leads to biofilm formation and colocalizes with matrix polysaccharides in the human pathogenic fungus *Aspergillus fumigatus*. *Front Microbiol.* 2013;4:141. <https://doi.org/10.3389/fmicb.2013.00141>.
49. Mesa-Grajales DH. Principles and applications of the Electron Back-Scattering Diffraction Tecnical (EBSD). [Principios y aplicaciones de la técnica de difracción de electrones retro-proyectados]. *Informador Técnico.* 2010;74:64–74; <https://doi.org/10.23850/22565035.9>.
50. Chen H, Yao Y, Warner JA, Qu J, Yun F, Ye Z, Ringer SP, Zheng R. Grain size quantification by optical microscopy, electron backscatter diffraction, and magnetic force microscopy. *Micron.* 2017;101:41–7. <https://doi.org/10.1016/j.micron.2017.06.001>.
51. Casas-López JL. Production of lovastatin from *Aspergillus terreus* in a fluidized bed reactor. PhD thesis, Universidad de Almería, 2004.
52. Hu Z, He B, Ma L, Sun Y, Niu Y, Zeng B. Recent Advances in Ergosterol Biosynthesis and Regulation Mechanisms in *Saccharomyces cerevisiae*. *Indian J Microbiol.* 2017;57(3):270–7. <https://doi.org/10.1007/s12088-017-0657-1>.

53. Singh S, Kaur H, Singh MM, Rudramurthy S, Chakrabarti A. *Aspergillus terreus* causing probable invasive aspergillosis in a patient with cystic fibrosis. *Mycopathologia*. 2019;184:151–4. <https://doi.org/10.1007/s11046-018-0294-1>.
54. Krishnamoorthy G, Kannan S, Marudhamuthu M. Bioactive compound from *Aspergillus terreus* DMTMGK004 synergistically contributes towards potential anti-pathogenicity. *Lett Appl Microbiol*. 2018;67:579–88. <https://doi.org/10.1111/lam.13071>.
55. Lass-Flörl C, Dietl AM, Kontoyiannis DP, Brock M. *Aspergillus terreus* Species Complex. *Clin Microbiol Rev*. 202;34(4):e0031120; <https://doi.org/10.1128/CMR.00311-20>.
56. Lass-Flörl C. Treatment of Infections Due to *Aspergillus terreus* Species Complex. *J Fungi (Basel)*. 2018;4(3):83. <https://doi.org/10.3390/jof4030083>.
57. Ramírez-Granillo A, Bautista-Hernández LA, Bautista-De Lucío VM, Magaña-Guerrero FS, Domínguez-López A, Córdova-Alcántara IM, Pérez NO, Martínez-Rivera MLA, Rodríguez-Tovar AV. Microbial Warfare on Three Fronts: Mixed Biofilm of *Aspergillus fumigatus* and *Staphylococcus aureus* on Primary Cultures of Human Limbo-Corneal Fibroblasts. *Front Cell Infect Microbiol*. 2021;11:646054. <https://doi.org/10.3389/fcimb.2021.646054>.
58. Blanchette RA, Biggs AR, editors *Defense Mechanisms of Woody Plants Against Fungi*. Springer Series in Wood Science. Berlin: Springer, 1992; <https://doi.org/10.1007/978-3-662-01642-8>.
59. Gašparíková O, Mistrík I, Čiamporová M, Waisel Y, Eshel A, Kafkafi U, editors. In: *Plant roots. The Hidden Half*, Edition: 3rd ed. Chapter: Sieber TN Fungal Root Endophytes. Publisher: Marcel Dekker, New York: pp. 887–917; <https://doi.org/10.1093/aob/mcf252>.
60. Ouellette GB, Baayen RP, Rioux D, Simard M. Peculiar ultrastructural characteristics of fungal cells and of other elements apposed to and in vessel walls in plants of a susceptible carnation cultivar, infected with *Fusarium oxysporum* f.sp. *dianthi* race 2. *Phytoprotection*. 2004;85(3):121–38. <https://doi.org/10.7202/010905ar>.
61. Padhi S, Uppin SG, Uppin MS, Umabala P, Challa S, Laxmi V, Prasad VB. Mycetoma in South India: retrospective analysis of 13 cases and description of two cases caused by unusual pathogens: *Neoscytalidium dimidiatum* and *Aspergillus flavus*. *Int J Dermatol*. 2010;49(11):1289–96. <https://doi.org/10.1111/j.1365-4632.2010.04610.x>.
62. Allkja J, Bjarnsholt T, Coenye T, Cos P, Fallarero A, Harrison JJ, Lopes SP, Oliver A, Pereira MO, Ramage G, Shirliff ME, Stoodley P, Webb JS, Zaat SAJ, Goeres DM, Azevedo NF. Minimum information guideline for spectrophotometric and fluorometric methods to assess biofilm formation in microplates. *Biofilm*. 2019;2:100010. <https://doi.org/10.1016/j.biofilm.2019.100010>.
63. Rodríguez-Tovar AV, Ruiz-Medrano R, Herrera-Martínez A, Barrera-Figueroa BE, Hidalgo-Lara ME, Reyes-Márquez BE, Cabrera-Ponce JL, Valdés M, Xoconostle-Cázares B. Stable genetic transformation of the ectomycorrhizal fungus *Pisolithus tinctorius*. *J Microbiol Methods*. 2005;63(1):45–54. <https://doi.org/10.1016/j.mimet.2005.02.016>.
64. Sangrador-Deitos MV, Olvera J, Espinal HA, Hernández GC, Morales VA, Soto Hernandez JL. Fungal mycotic aneurysm in a patient with *Aspergillus terreus* chronic meningoencephalitis. *Surg Neurol Int*. 2020;11:139. [https://doi.org/10.25259/SNI\\_506\\_2019](https://doi.org/10.25259/SNI_506_2019).



# Table

**Table 1. Results of morphological description of *A. terreus* biofilm formation by SEM-HR**

Biofilm establishment period	Characteristics of fungal biofilm						Stage
	ECM	Hyphae	Anastomosis	Conidia	Aerials channels	Microhyphae	
24 h	+++	+++	+++	++	✓	✓	Early maturation
48 h	++	++	++	-	✓	-	Depletion
72 h	++++	++++	++++	-	✓	-	Late maturation
96 h	+	+	+	++++	✓	-	Dispersion

\* (ECM): Extracellular matrix; (h): hours; (+): proportion of observed characteristics; (✓): these structures were observed; (-): these structures were not observed.

# Figures

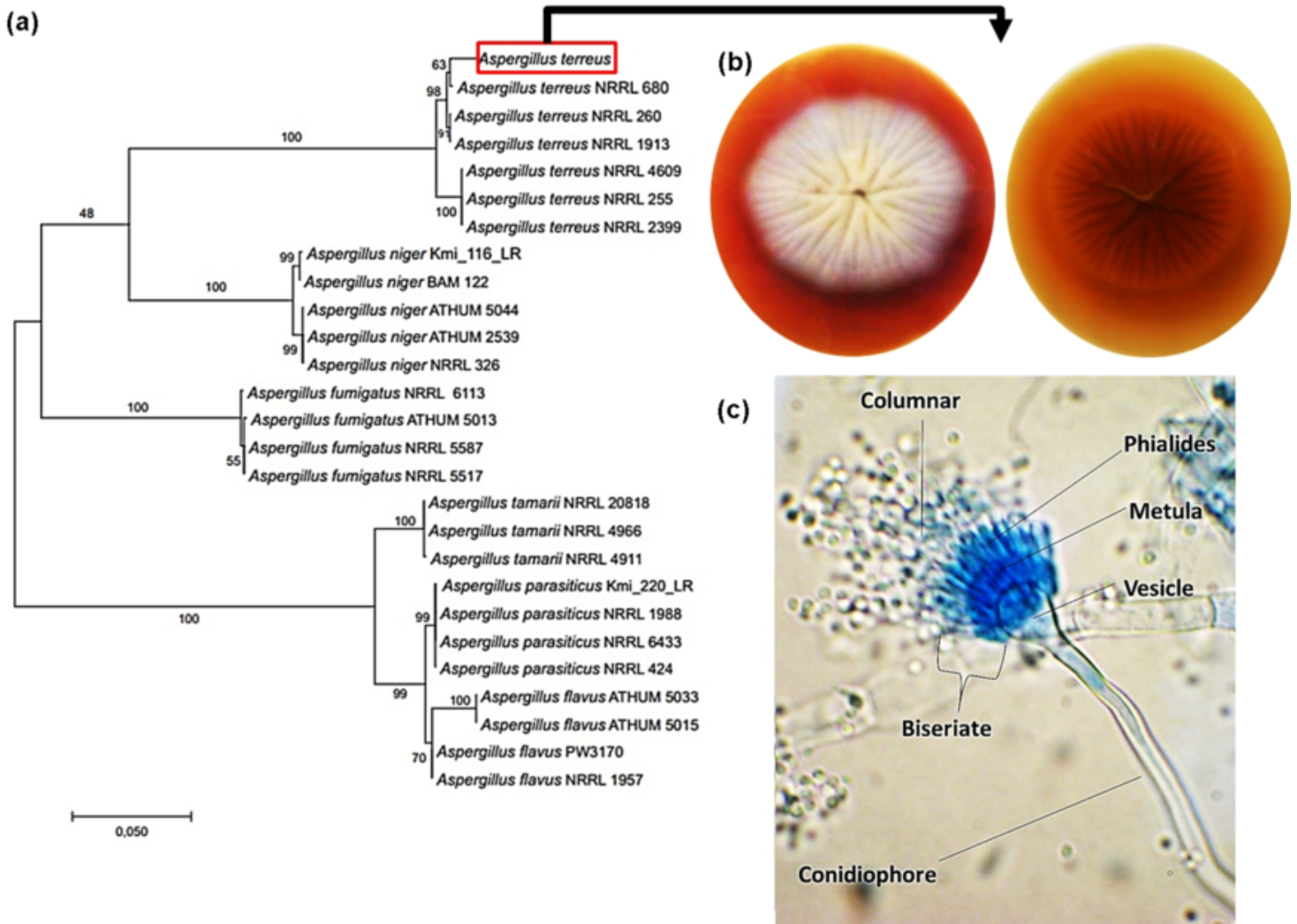


**Figure 1**

**Molecular and microbiological identification of the cerebral clinical isolate of *A. terreus*.** a) Molecular identification: The phylogenetic tree of maximum likelihood elaborated shows the relation of the molecular markers for filamentous fungi that were used (ITS and RPBII), with some sequences of *Aspergillus* species obtained by BLAST. b) Microbiological identification. *A. terreus* was grown on PDA at 37°C/48 h; Colonial morphology: powdery texture, cinnamon-brown color, front (left) and back (right). c) Microscopy observation: Conidial head, metula and phialides with conidium emerging in columnar form (100x; lactophenol cotton blue stain).

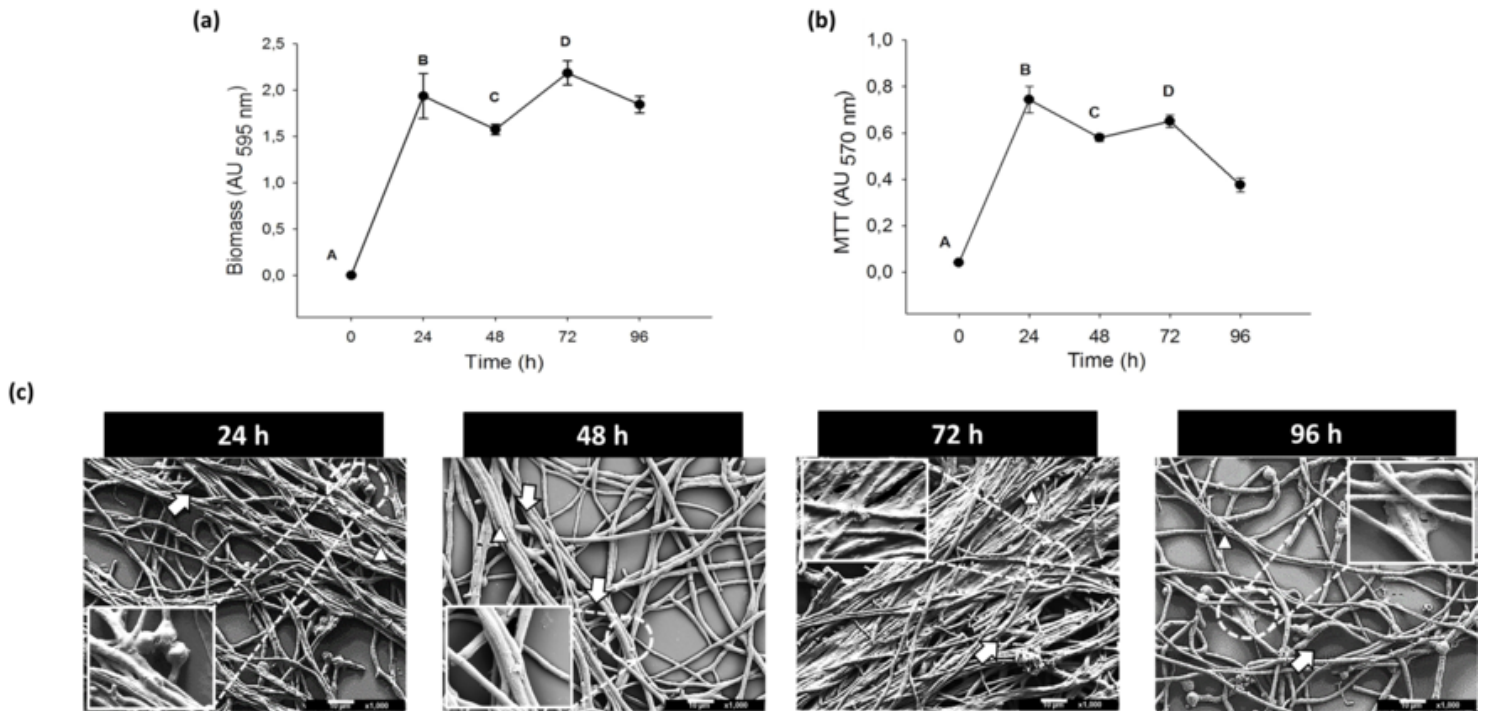


**Figure 2**

***A. terreus* biofilm, quantification (CVM and MTT) and observation by SEM-HR.** Biofilms were made with RPMI at  $4 \times 10^5$  conidia/mL at 37°C during 0 to 96 h. The quantification was done for two methods: (a) Method of Christensen with crystal violet 0.005%. (b) Method of reduction of tetrazolium salts with MTT 0.3%. Student Neumals Kewls was used as statistical method with  $n = 12$ . The letters represents the value of  $p < 0.05$  (A: 0 and 24; B: 24 and 48; C: 48 and 72; D: 72 and 96) for both methods. (c) Images by SEM of *A. terreus* biofilm 24 h (a), 48 h (b), 72 h (c) y 96 h (d). Presence of exopolymeric substance on the hyphae (zoom, x5000), channels formation (arrow) and hyphae fusion (arrowhead).

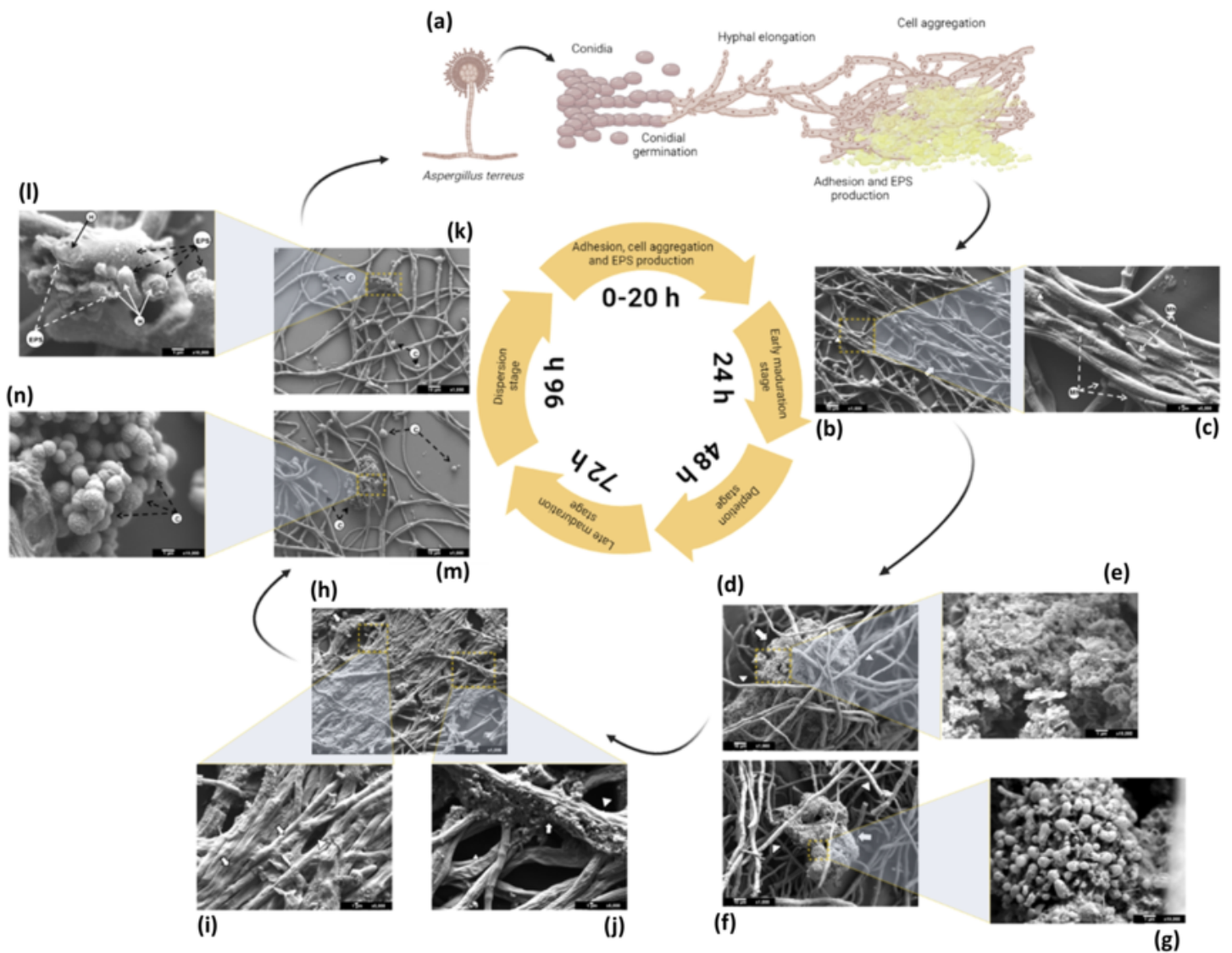


**Figure 3**

**Stages of the biofilm formation cycle of the clinical brain isolate of *A. terreus*.** The biofilm was grown in RPMI at 37°C. The micrographs were made by SEM-HR. (a) Establishment during the first hours of the filamentous fungal biofilm was described as processes of adhesion, cell aggregation, EPS production and development of biofilm formation. **24 h**) During the early maturation stage, the presence of anastomosis (arrowhead) and the formation of canals (arrow) were observed (b, x1000). Also, evidence of the presence of microhyphae (Mh) was observed in the developed hyphae (c, x5000). **48 h**) In depletion phase, a wider ECM with embedded hyphae (arrowhead) was present (d, x1000). In some fields, a type of ECM (arrow) with both condensed and porous type consistency was visible. In addition, some artifacts with an apparently waxy consistency were observed (e, x10000). In another field, a porous-type ECM with globular structures at the periphery was observed (f, x1000; g, x5000). **72 h**) At late maturation stage, we observed the highest ECM formation (h, x1000). In the same field was evidenced the presences of a condensed ECM and film ECM (i, x5000). While in other fields porous ECM was detected (j, x5000). Anastomosis (arrow); fungal channels (arrowhead). **96 h**) The dispersion phase showed a significant decrease in biofilm formation. Accumulation of exopolymeric substances was also observed (k, x1000). An amorphous substance covered by a layer of

ECM coating the hyphae was evident (l, x10000). In some fields, sparse remains of conidia were found (m, x1000), which were coated with exopolymeric material adjacent to the hyphal growth of the fungus (n, 10000). Conidia (c); hyphae (h); exopolymeric substances (EPS).

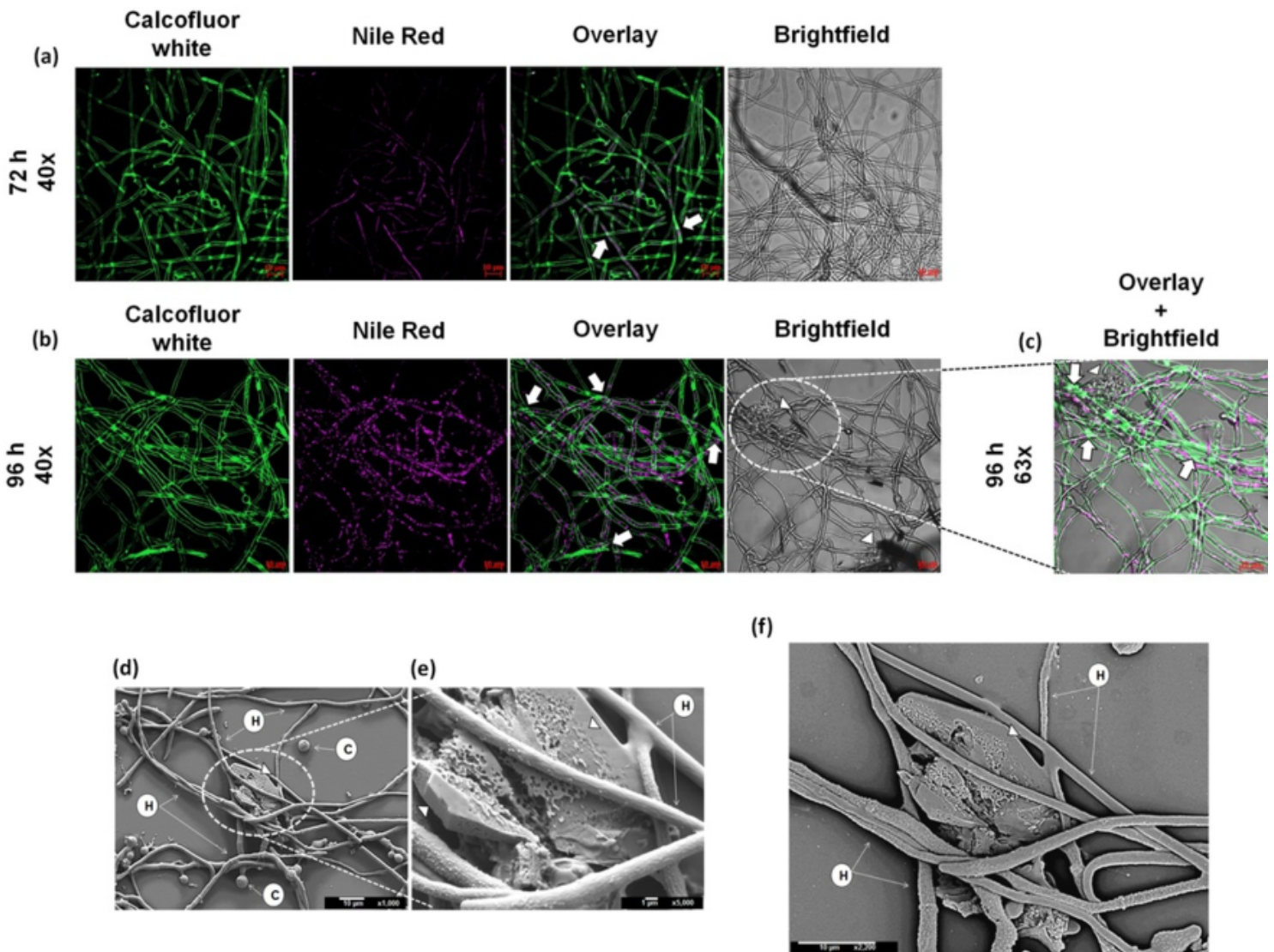


**Figure 4**

**Lipid detection of *in vitro* biofilm in a clinical brain isolate of *A. terreus*.** The biofilm was cultured in RPMI at 37°C. Lipid analysis of the fungal biofilm was performed by CLSM and SEM-HR with backscatter-electron diffraction. **CLSM**) The lipid was detected outside the hyphae at about 72 h after biofilm formation (a, 40x). Compared to the earlier period, at 96 h an increased presence of lipids was observed in the peripheral hyphae (b, 40x). Further, in magnified detail, lipid clusters were observed in coexistence with carbohydrates bound to an ECM (c 63x). Calcofluor white (chitin-green halo) and Nile red (lipid-pink halo) were used as fluorochrome markers. **SEM-HR**) The waxy ECM was surrounded by hyphae (d, 1000x), and at higher magnification; a faceted form with waxy consistency secreted by the hyphae could be discerned (e, 5000x). SEM with backscatter-electron diffraction was used to differentiate the waxy material originating from the ECM secreted by the fungus (f, 2200x). Molecular co-localization of lipids (white arrow); presence of ECM (white arrowheads); hyphae (H); and conidia (C).

## Supplementary Files

This is a list of supplementary files associated with this preprint. Click to download.

- [ESM1.pdf.pdf](#)